Nanoscale Advances

ROYAL SOCIETY OF CHEMISTRY

PAPER

View Article Online
View Journal | View Issue



Cite this: *Nanoscale Adv.*, 2022, **4**, 4895

# Partially oxidised boron nitride as a 2D nanomaterial for nanofiltration applications†

Natalia García Doménech, [ab] Áine Coogan, [a] Finn Purcell-Milton, [abc] María Luisa Casasín García,[a] Adrián Sanz Arjona, [a] Marc Brunet Cabré,[a] Aran Rafferty, [a] Kim McKelvey, [d] Peter Dunne [a] and Yurii K. Gun'ko *[ab]

Boron nitride (BN) based 2D nanomaterials are an emerging class of materials for the development of new membranes for nanofiltration applications. Here, we report the preparation, characterisation and testing of highly promising nanofiltration membranes produced from partially oxidised BN (BNOx) 2D nanosheets. In our work, the partial oxidation of BN was successfully achieved by heating the bulk h-BN powder in air at 1000 °C, resulting in BNOx product. The characterisation of the sample showed the presence of B–OH groups corresponding to the partial oxidisation of the BN. The BNOx material was then exfoliated in water and used to produce membranes, using vacuum filtration. These membranes were characterised using electron microscopy, BET and mercury porosimetry techniques. The membranes have also been tested in water purification and removal of several typical water-soluble dyes, demonstrating outstanding retention values close to 100%. We believe that this research opens up new opportunities for further production, as well as chemical functionalisation and modification of membranes for nanofiltration and separation technologies.

Received 20th July 2022
Accepted 24th October 2022

DOI: 10.1039/d2na00472k

rsc.li/nanoscale-advances



## 1. Introduction

Access to clean water has become increasingly scarce in recent years due to various factors, such as increasing population density, urbanisation, and inequality, among others.[1] The development of new, inexpensive, and reliable methods for the removal of various impurities and toxins from water is therefore vital. In recent years, the emergence of nanofiltration (NF) membranes has become an exciting prospect for water purification. NF can be described as a type of filtration which exhibits separation characteristics in between reverse osmosis and ultrafiltration, and typically has molecular weight cut-offs in the region of 200–1000 Daltons.[2,3] Various nanomaterials have been implemented in NF membranes, such as metal organic frameworks (MOFs), metal oxide nanoparticles and nanotubes.[4–6] NF membranes based on 2D nanomaterials such as graphene and boron nitride (BN) have attracted significant interest due to the unique properties of 2D nanomaterials, most importantly their high surface-to-volume ratio, which leads to high adsorption capacity. In particular, BN is an attractive candidate for use in NF membranes as it is mechanically strong, inexpensive, and environmentally friendly. BN-based membranes have been the subject of numerous studies, with BN shown to be very effective in the removal of several water pollutants, including various dyes, that often can be leached into wastewater, from the textile industry.[7–9]

Boron nitride (BN) is very stable, both chemically and thermally, which can act as a barrier to its functionalisation, as harsh chemical reactions are often needed. Due to the similar characteristics of BN and graphene, the oxidation of BN as an analogue to graphene oxide (GO) is an area of significant interest. The main barrier to BN oxidation is its high thermal resistance,[10] which means that the chemistry commonly used for GO doesn't work for BN. However, the introduction of oxygen in the BN structure is still under investigation.[11,12]

One of the potential approaches to change the properties of hexagonal BN (h-BN) is to carry out elemental doping. Some theoretical studies have suggested that oxygen may be able to alter the properties of h-BN when acting as a dopant.[12] Oxygen, once inserted into the BN lattice, has the capability to decrease the h-BN bandgap, making the material more conductive.[12–15] It can also regulate molecular interactions[12,16,17] and cause some strong spontaneous magnetization.[12–14] Some recent experimental works have supported these theoretical simulations.[12,18–20] There are several reports on the physical and chemical effects that introducing oxygen has on the h-BN

[a]*School of Chemistry, Trinity College Dublin, D02 PN40, Dublin, Ireland. E-mail: igounko@tcd.ie*

[b]*BiOrbic, Bioeconomy Research Centre, University College Dublin, D04 V1W8, Dublin, Ireland*

[c]*School of Chemical and Pharmaceutical Sciences, Technological University Dublin, D07 H6K8, Dublin, Ireland*

[d]*School of Chemical and Physical Sciences, Victoria University of Wellington, Wellington 6012, New Zealand*

† Electronic supplementary information (ESI) available. See DOI: https://doi.org/10.1039/d2na00472k

structure. The signature peak of h-BN in Raman has been shown to broaden due to the oxidation of the material,[12,21] indicating a possible change in the crystal domain size, amorphization or disordering.[12,21] The improvement of the production of BN nanosheets (BNNs) has been reported, due to the oxidation of h-BN.[12,22] However, the exact mechanism of how oxygen doping affects the exfoliation of h-BN is still poorly understood. Furthermore, the addition of oxygen atoms could cause a distortion to the structure of the h-BN sample.[12,20]

When it comes down to experimental work, BNNs functionalised with hydroxyl groups (OH-BNNs) can be obtained using several different methods. Some of these methods include heating bulk h-BN in air,[10,11] treating BN powder with a hot solution of $H_2SO_4$/$KMnO_4$ [11,23] or functionalisation by oxygen radicals, followed by hydrolytic defunctionalisation.[11,24] The surface energy of the BNNs, as well as their solubility in various solvents, can be altered as a result of the introduction of these OH groups.[11] Hydroxyl groups, as they are very common in nature, can interact with many different types of organic and inorganic materials. Thus, BNNs exciting properties can be further exploited by inserting OH groups to the structure.[11]

One of the most effective and straightforward ways of introducing oxygen and OH groups into h-BN is *via* heating under air.[12] Treating h-BN with high temperatures (800–1000 °C) in an air environment is capable of introducing oxygen into the structure of the 2D material. The mechanism of hydroxyl functionalisation in BN, while not yet fully understood, has been reported to occur at the boron edge sites of the BN structure. The introduction of oxygen displaces preferentially the nitrogen atoms, forming covalent bonds with the boron atoms at the edges of the nanosheets.[12,25]

As a result of the introduction of these hydroxyl groups due to the oxidation of BN, oxidised BN (BNOx) is more reactive than its parent material, that also allows further functionalisation of the material.

# 2. Experimental

## 2.1. Starting materials

Hexagonal boron nitride (h-BN) powder was purchased from Merck (particle size = 6–30 μm). Evans Blue (≥75%) and Methylene Blue (≥82%) were obtained from Sigma-Aldrich. Methyl Orange (≥95%) was bought from VWR international Ltd. Millipore Water was obtained using a Milli-Q system, with resin filters; this filtration was carried out in Trinity College laboratories. Durapore membrane filter (hydrophilic polyvinylidene fluoride, PVDF, with 0.45 μm pore size and 47 mm diameter) were purchased from Merck Millipore Limited. The sonic bath used was Ultrawave model U100H from Ultrawave Ltd.

## 2.2. Preparation and exfoliation of BNOx

Bulk BN was oxidised by heating in a furnace in an air atmosphere. The temperature of the oven was increased 5 °C per minute and the temperature was kept at a 1000 °C for 30 min, producing the oxidised BN (BNOx). The BNOx was obtained, and the material was exfoliated following the methods described previously for BN.[26]

## 2.3. Preparation of membranes

The membranes were prepared following the procedure described by García Doménech *et al.*[26] A 50 mL solution containing 150 mg of exfoliated BNOx was deposited by vacuum filtration on top of a PVDF template with a pore size of 0.45 μm.

## 2.4. Characterisation

Powder X-ray diffraction (XRD) was carried out on a zero-background holder using a Bruker D2 Phaser 2nd Gen. Measurements were performed for $2\theta$ between 10 and 80, with no fluorescence correction and a $2\theta$ increment of 0.01 per second. Scanning electron microscopy (SEM) images were obtained using a Zeiss Ultra Plus Scanning Electron Microscope. UV-Vis spectra were recorded using a Cary 60 spectrophotometer with a wavelength between 200 and 800 nm. AFM measurements were carried out on a Park NX10 (Park Systems, Suwon, South Korea). The AFM images were obtained in a non-contact mode (NCM) with a PPP-NCHR cantilever type (force constant of 42 N $m^{-1}$ and resonance frequency of 330 kHz, Nanosensors). Single BNOx flakes were deposited for AFM analysis by drop casting 0.03 mg $mL^{-1}$ of exfoliated BNOx solution on gold-coated glass slides purchased from Evaporated Metal Films (TS-TA-134). Brunauer–Emmett–Teller (BET surface area analysis was performed using a Nova 2400e Surface Area Analyser (Quantachrome, Hampshire, UK). Membranes were cut to size using a blade. Prior to analysis, samples were degassed for 6 h at 200 °C under vacuum. The BJH method was used to calculate the pore size diameter and pore volume from the desorption branch of the isotherms. The BJH values presented here include pores in the range of 1–30 nm. Mercury porosimetry was performed using an Autoscan-33 Porosimeter (Quantachrome, Hampshire, UK) with a default contact angle of 140°. Raman spectra were recorded using a Renishaw Raman Microscope with a 785 nm laser, equipped with three lenses and an automated xyz stage. The measurements were taken using the laser at 100% power with an exposure of 60 from 1600 to 1100 $cm^{-1}$. The FT-IR spectra were recorded using a PerkinElmer Spectrum 100 with PerkinElmer Universal ATR Sampling Accessory. It consists of 4 recording iterations collected, summed and averaged. The full spectra wavelength range was from 4000 $cm^{-1}$ to 500 $cm^{-1}$ in steps of 2 $cm^{-1}$. Thermogravimetric analysis (TGA) measurements were carried out under air atmosphere, using a PerkinElmer Pyris 1 TGA, and 3.5 mg of solid sample in a ceramic crucible.

## 2.5. Retention tests

Three water soluble dyes were selected for testing the membrane retention: Evans Blue, Methyl Orange and Methylene Blue. The concentrations were chosen based on the maximum of absorbance, which was between 1 and 1.5 au, as seen in Table S1† and matches with concentration used in literature.[27]

20 mL of the dye solution were passed through the membrane and a UV-Vis spectrum of the permeate was recorded. Once the permeate was obtained, further concentration of it was required, to collect an adequate UV-Vis spectrum. To do this, a rotary evaporation was carried out until only solid matter was present. 3 mL of Millipore water were then added, and the absorbance of this concentrated solution was measured using an UV-Vis spectrometer.

The following formula was used to calculate retention, as has been used in our previous work:[26]

$$R_x\ (\%) = \left(1 - \frac{A_{P,\lambda_{max}}}{A_{F,\lambda_{max}}}\right) \times 100$$

where: $R_x$ is the retention in percentage, $A_{F,\lambda_{max}}$ is the absorbance at $\lambda_{max}$ of the analyte in the feed, $A_{P,\lambda_{max}}$ is the absorbance at $\lambda_{max}$ of the analyte in the permeate.

The statistics of the retention were calculated using Origin software 2018.

Water permeance (flux) experiments were carried out by passing 20 mL of the analyte through the membrane, while the operating pressure of the filtration system was kept at 1 bar. Flux values were calculated according to the following formula as reported by Chen *et al.*[8]

$$F = \frac{V}{At}$$

where: $F$ is the flux in L m$^{-2}$ h$^{-1}$, $V$ is the volume of analyte in L, $A$ is the working area in m$^2$, $t$ is the time taken for the analyte to pass through the membrane (in h). The working area of the filtration system is 9.6 cm$^2$.

## 3. Results and discussion

### 3.1. BN oxidation and exfoliation

BN was oxidised by heat treatment at 1000 °C for 30 min under air in a tubular furnace, to introduce OH groups into the h-BN structure. It has been previously reported by Andriani *et al.* that treatment of h-BN in this manner leads to the formation of hydroxyl groups, which tend to form on the edges of the h-BN layers.[12] The BNOx product was initially characterised by XRD and FT-IR (Fig. 1).

The XRD (Fig. 1A) pattern shows the characteristic peaks corresponding to BN, showing high crystallinity.[28,29] In addition, we can observe a new peak at $2\theta = 27.7°$ (010) corresponding to $B(OH)_3$,[12,30] as well as an additional $B(OH)_3$ associated reflection at 14.6°, both of which seem to indicate that oxidation/hydroxylation has taken place (JCPDS 30-0199). Furthermore, FT-IR was also carried out for the BNOx and compared to that of the parent material, h-BN (Fig. 1B). FT-IR spectra of both BN and BNOx show the peaks corresponding to B–N bending, around 769 cm$^{-1}$ and B–N stretching at 1344 cm$^{-1}$, characteristic of BN.[12] In BNOx, an additional peak is present at around 1190 cm$^{-1}$, due to the splitting of the 1344 cm$^{-1}$ peak, that can be attributed to the B–O bonds.[31] In addition, a new peak emerges in the 3200 cm$^{-1}$ region corresponding to the B–OH stretching vibrations.[12] Additional peaks at 883 cm$^{-1}$ and 636 cm$^{-1}$ are due to B–O stretching vibrations and B–O bending vibrations, respectively.[12] These peaks are evidence of the successful oxidation of BN *via* heating.

TGA was also carried out on bulk h-BN using a ramp rate of 5 °C min$^{-1}$ and a temperature range of 25 °C to 900 °C, to simulate the process of oxidation in the furnace (Fig. 2A). Due to limitations of the instrument, the TGA curve was only recorded up to 900 °C, as the 30 minute high-temperature holding step may have led to damage of the thermocouple at 1000 °C.

The TGA curve shows an overall increase of roughly 3% in the mass of the sample. Derivative analysis of the TGA curve reveals a sharp increment in weight which occurs around 720 °C, followed by a steady increase in mass with the rise in temperature, until it stabilises with the holding of the temperature at 900 °C. This increase in weight likely corresponds to the addition of the OH groups to the edges of the sheets.[12] As has been reported in literature, the increase in temperature results in a higher number of OH groups being formed at the BN layer edges,[12] which can be correlated to the increment in weight that is observed in the TGA curve shown here. FT-IR was also conducted after the TGA was completed (Fig. 2B) and confirms the oxidation of the BN. The FT-IR spectra shows the appearance of the peak at 1190 cm$^{-1}$, that as previously mentioned can be

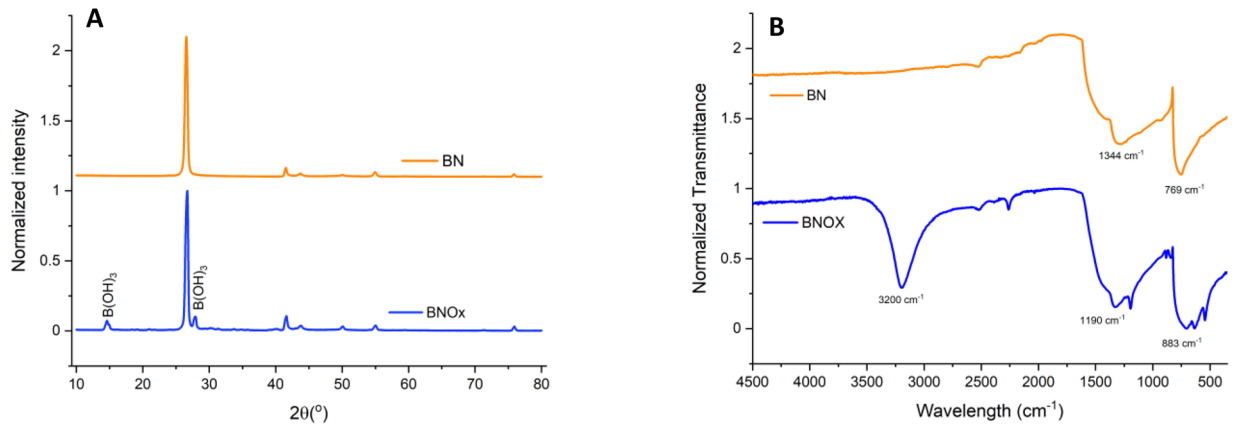


Fig. 1 (A) XRD patterns and (B) FTIR spectra of BNOx (blue) and BN (orange).

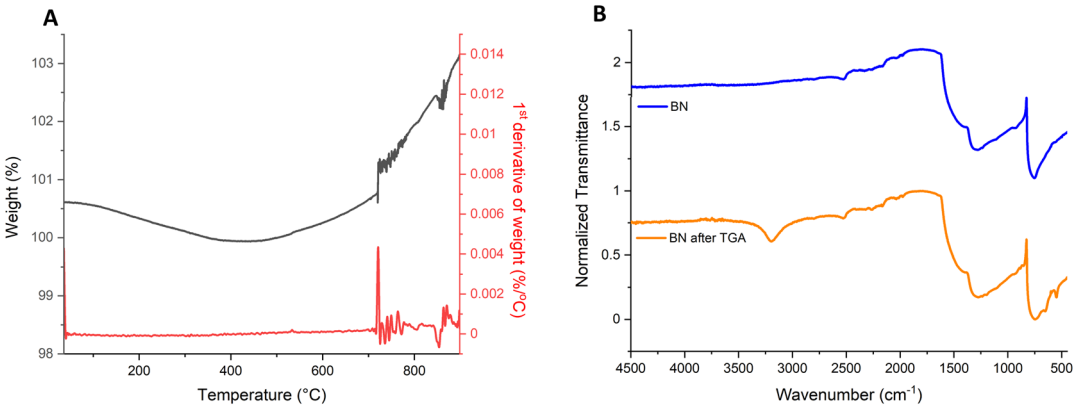


Fig. 2 (A) TGA and differential TGA of bulk h-BN to monitor the oxidation and (B) FT-IR of the BN after running TGA compared to h-BN.

attributed to the B–O bonds,[31] the 3200 $cm^{-1}$ peak corresponding to the B–OH stretching vibrations,[12] the 883 $cm^{-1}$ peak due to B–O stretching vibrations and a final peak at 636 $cm^{-1}$ attributed to B–O bending vibrations.[12] These peaks are proof of the successful oxidation of BN *via* heating.

Zeta potential (ζ) measurements were also carried out on exfoliated BNOx and compared with exfoliated h-BN, in order to see if there was negative charges appearing in the oxidised BN, as a result of the OH groups present. Exfoliated h-BN shows only a small ζ of −5.29 mV (Fig. S1†). However, exfoliated BNOx displays a strong negative average potential of ζ = −44.7 mV (Fig. S1†). The ζ plot of BNOx displays two peaks, one at −32.8 mV and the other at −52.9 mV. This strongly negative surface charge of the oxidised BN is due to the presence of OH groups on the surface and is further proof of successful oxidation of the BN *via* this simple heating method.

After the heat treatment of the BN in order to produce BNOx, it was observed that on some occasions, the product can be produced in two forms. Part of the BNOx would appear as a powder, similar to BN, while the rest will form "rocks" that were hard and difficult to break (Fig. S2†). The powder appeared at the top of the sample, whereas the rocks were found toward the bottom and sides of the vessel, mixed in with the powder.

FT-IR and XRD (Fig. S3†) of the two samples (powder and rocks) did not reveal any major changes between the two. Overall, the peaks that could be identified due to the presence of BN and partially oxidised BN were present (as described in Fig. 1). There were more peaks appearing in the case of the rocks in the areas of $H_3BO_3$, B–N and $NH_2$ and NH bonds, which could indicate differences in the vibration of the bonds. This could be associated to the different morphology, while the compound remains the same form, partially oxidised BN. This has been reported previously by Andriani *et al.*[12] where they noted the sample heated at 1000 °C was the hardest and had to be ground for further use. This would be very similar to the formation of the rocks in this case, where the rocks are formed most likely due to agglomeration of the powder in the furnace as a result of different heating (sides and bottom *vs.* top of the sample). Hydrogen bonds can be formed in layered materials with hydroxyl groups, like graphene oxide[32] or clays.[33] High temperature treatment, as it has been done here, results in samples rich in hydroxyl groups, which could form hydrogen bonds. These strong hydrogen bonding may facilitate the clustering of BNOx, forming these rocks.[12]

BNOx was then sonicated for 24 hours in Millipore water to obtain the exfoliated material, in-line with our previous work, as this solvent was the one that gave the best performance membranes after the exfoliation.[26] It was noted that when using the BNOx as rocks, even though they are quite hard and difficult to break, this sample was completely dispersed in water after exfoliation. Therefore, the powder and rocks were both used for membrane formation, as there was no distinct differences between the two forms as previously mentioned. UV-Vis of the BNOx solution was taken and compared with bulk BN and exfoliated BN (Fig. 3).

UV-Vis absorbance spectra of BNOx did not show any differences with that of the exfoliated BN, displaying the same shape. The difference in the absorbance is likely due to a different concentration. Both samples are easily differentiated from bulk BN dispersed in water.

XRD and FT-IR of the exfoliated BNOx were also carried out to check whether the exfoliation has an effect on the oxidation/hydroxylation of the BN (Fig. 4). The XRD pattern of the

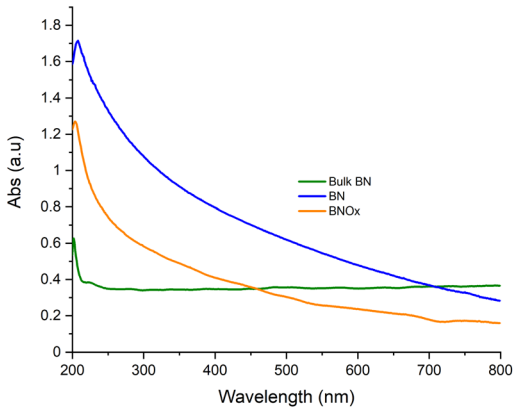


Fig. 3 UV-Vis spectra of bulk BN (green), exfoliated BN (blue) and exfoliated BNOx (orange).

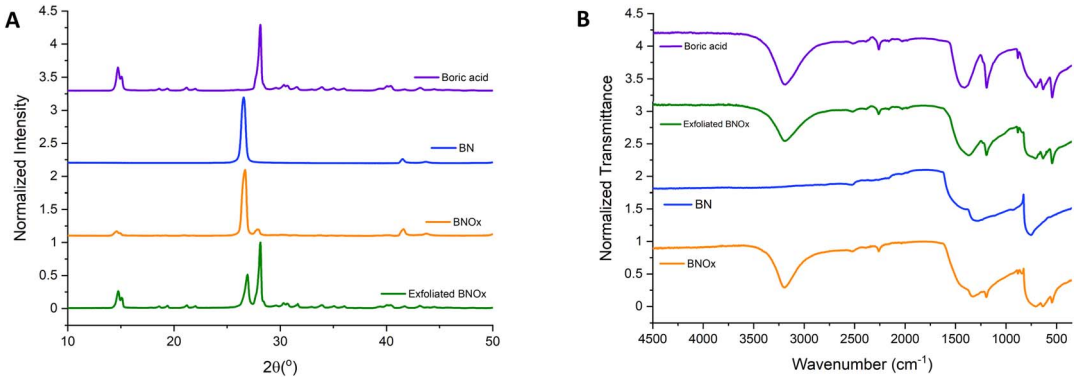


Fig. 4 (A) XRD patterns and (B) FT-IR spectra of boric acid (purple), BN (blue), BNOx (orange) and exfoliated BNOx (green).

exfoliated BNOx samples shows the peaks corresponding to the oxidation/hydroxylation are more prominent than in the case of bulk BNOx. The peaks for $B(OH)_3$ are more intense than the BN peaks, which indicates that there is a higher degree of oxidation after the exfoliation in water. The stronger peaks in the exfoliated BNOx can be matched to boric acid (purple in the graph). One possible explanation for this is that the introduction of OH in the structure through the heating process results in the formation of more OH groups at the surface of the BN during the exfoliation, due to sonication-assisted hydrolysis.[34] The use of steam at the same time as heating has been previously reported,[11] but the amount of hydroxylation was smaller than the one observed by heating h-BN at 1000 °C following by 24 hours of sonication in water. The FT-IR also shows some differences between the exfoliated BNOx and bulk BNOx, with the peaks at 1344, 1190, 883 and 636 $cm^{-1}$ becoming sharper and more defined in the exfoliated sample, which further proves the higher level of hydroxylation of the BN thanks to the combination of heat and sonication in water. The peak at 540 $cm^{-1}$ is clearer in the exfoliated BNOx than the bulk BNOx. The FT-IR of the exfoliated BNOx is very similar to the FT-IR obtained when measuring boric acid, which further proves that degree of oxidation of the sample increases under sonication in water.

SEM images of the BNOx were taken after exfoliation to study the morphology of the nanosheets. These are shown in Fig. 5. SEM images of the nanosheets of the BNOx show no major differences with regular exfoliated BN, indicating that the oxidation doesn't change the shape of the nanosheets, which would make the BNOx a good candidate for membranes, as it would allow further functionalisation of the membranes while keeping the high-performance properties of the membranes. However, the size of the nanosheets was calculated to be 0.76 ± 0.3 μm (Fig. S4†), which is around 0.2 μm bigger than those nanosheets obtained when exfoliating regular BN.[26]

Raman of the bulk and exfoliated BNOx was also carried out and compared to that of bulk BN (Fig. 6). The Raman spectra show the $E_{2g}$ peak, with a bibliographic value of 1366 $cm^{-1}$.[35]

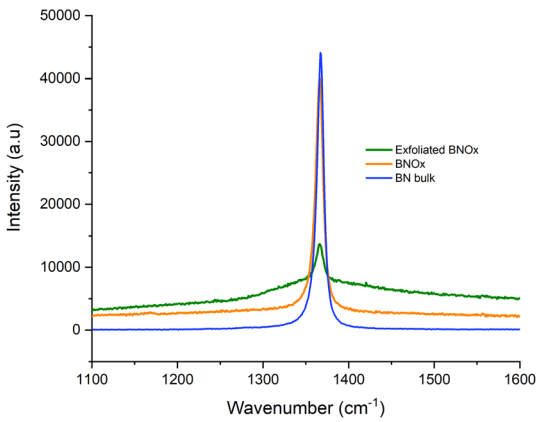


Fig. 6 Raman spectra of bulk BN (blue), BNOx (orange) and exfoliated BNOx (green).

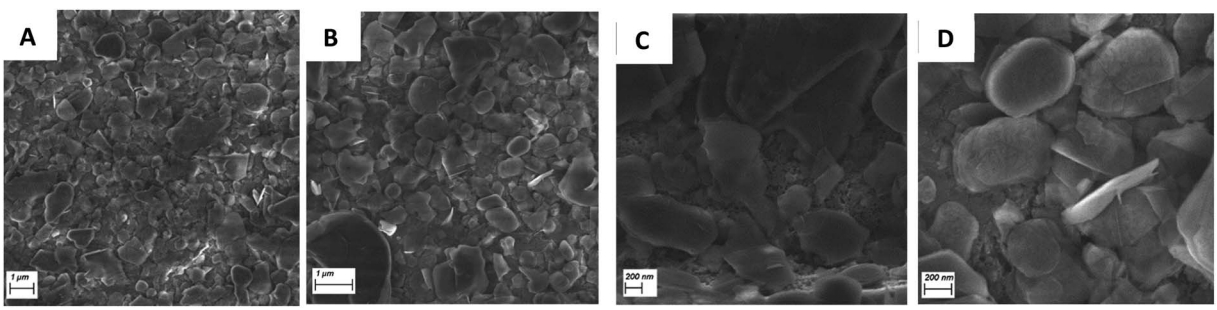


Fig. 5 SEM images of BNOx nanosheets after exfoliation. (A and B) Showing a general view and (C and D) showing a closer view of the nanosheets using InLens and EHT 3.0 kV.

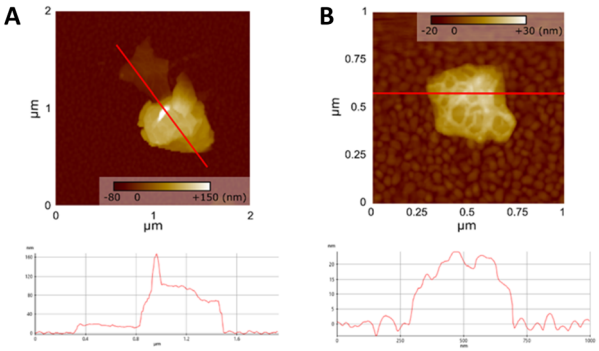


Fig. 7 AFM images of BNOx (A) nanosheets and profile and (B) single BNOx nanoflake with its profile.

Two key features can be observed in the spectra. The first one is that, as in the case of exfoliated BNOx *vs.* bulk BNOx, the exfoliated BNOx shows a decrease in the intensity of the peak of 65% when compared to the bulk BNOx peak. This is due to the reduction of layer thickness in the structure. In contrast with the exfoliated BN, no shift of the peak was observed (Table S2†). There is a clear broadening of the peak when BNOx is exfoliated and, to a lesser degree, with bulk BNOx also. This has been previously reported in literature by Li *et al.*, where the broadening of the peak is attributed to the oxidation of the material.[36] Furthermore, this broadening, larger in the case of the exfoliated BNOx, is also due to the exfoliation process.

AFM of the exfoliated BNOx was also carried out and it is shown in Fig. 7. AFM images of the flakes, as seen in Fig. 7A, shows that they are thicker than pure BN nanoflakes, being more than 100 nm of height. Most of the flakes present in the sample were over 100 nm in height, which makes the AFM analysis more difficult. However, there were some thinner nanoflakes present in the sample, which were chosen for analysis, as the one shown in Fig. 7A. These thinner nanosheets show a different morphology than the ones observed in the regular BN nanosheets, that had less "peaks" and were more uniform. Furthermore, in Fig. 7B, which shows a single BNOx nanosheet, it is easy to see that the nanosheet is not smooth, showing some roughness on the surface of the nanoflake. This is probably due to the effect of the oxide layer present in the nanoflake.

### 3.2. Preparation and investigation of BNOx based membranes

Exfoliated BNOx was used to fabricate membranes, using vacuum filtration as is commonly used for 2D nanomaterial-based membranes, and is described in our previous work.[26] The exfoliated BNOx solution looked very similar to the exfoliated BN one, with no major differences observed. The production of the membranes was also very similar to the BN membranes, with the process being identical for both samples.

These membranes were characterised using SEM, BET and mercury porosimetry and their performance was tested using several dyes.

Visual inspection of the membranes showed no differences with those obtained using regular BN (Fig. S5†). SEM images of the resulting membranes including both from top-view and from cross-section are shown in Fig. 8. Top-view SEM images (Fig. 8D) of the membranes showed no major differences from the regular BN membranes, with the nanosheets clearly visible. The membranes looked very similar to the BN ones, indicating that the oxidation of the BN doesn't affect the formation of the membranes, which should make the membranes have similar if not equal performances to those obtained from pure h-BN.[26] The cross-section profiles of the membranes (Fig. 8E–H)

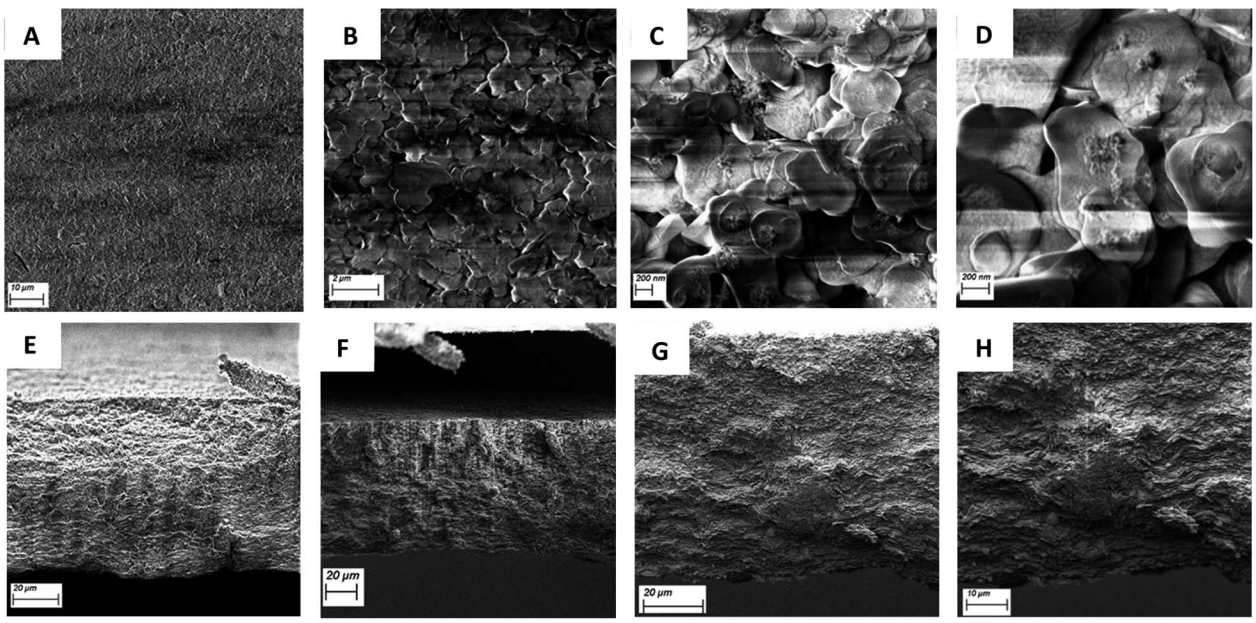


Fig. 8 SEM (A and B) top view and (C and D) closer view of the top-view of BNOx using InLens and EHT: 2.50 kV. (E–H) figure: SEM cross-section of the BNOx membranes using InLens and EHT: 2.50 kV.

showed the nanosheets tightly packed across the membranes. The thickness of the membrane was measured as 81 ± 4 μm, which is significantly thinner than the values obtained for the previously reported BN membranes (140–170 μm).[26] This more compact structure could have an effect on the performance and characteristics of the membranes.

Mercury porosimetry of the BNOx membranes was performed. The intrusion of mercury (Fig. S6A†) shows that these membranes have smaller pores than those found in BN membranes.[26] In terms of pore volume, the results obtained show similar values, with BN having 0.56 $cm^3$ $g^{-1}$ and BNOx 0.51 $cm^3$ $g^{-1}$. Although the values are very similar, the trend follows the one observed with the pore size, as the BNOx shows a smaller pore volume than BN. When observing pore size distributions, (Fig. S6B†), both materials have a broad peak initially followed by a second peak, corresponding to 54 nm for BN[26] and 44 nm for BNOx. In both cases, the BNOx curve is shifted to the right, which corresponds to smaller pore sizes.

BET was also carried out and the results are displayed in Table S3.† A major difference between pure BN and BNOx membranes was the pore diameter, with BNOx exhibiting larger values (22.6 nm *vs.* 3.5 nm for h-BN), around an order of magnitude higher. This difference is most likely due to the smaller pore sizes for BNOx, as it falls closer within the BET range. However, in terms of surface area, no difference can be observed, as both values are almost identical. This can be explained by the fact that BNOx has larger pore diameter and pore volume, but since these two cancel each other out, the surface area would be similar to the BN one.[26]

### 3.3. Retention and flux studies of BNOx membranes

The BNOx-based membranes were then tested using the same dyes used to test the BN membranes in previous reports.[26] Initially, BNOx membranes were initially tested for retention of Evans Blue dye. The UV-Vis absorption spectra of the Evans Blue permeates after passing through the as-prepared BNOx membranes are shown in Fig. 9. The retention of the BNOx membranes was 99% ± 1 (data is shown in Table S4†), which is very similar to those observed for the original BN-based membranes.[26] This further proves that the oxidation of BN does not affect the formation or performance of the membranes. An image of a membrane after filtering Evans Blue is shown in Fig. S7† and shows the clear staining of the membrane due to retention of the dye. The solvent transport properties of the membranes were also investigated. The permeance was calculated, both for pure (Millipore) water, and for the Evans Blue analyte. On average, the permeance of pure water was calculated to be 1163 L $m^{-2}$ $h^{-1}$, whereas when Evans Blue solution was passed through the membrane, a slightly lower flux of 677 L $m^{-2}$ $h^{-1}$ was observed, which is quite high for a membrane of this thickness. The flux values obtained in this study are in line with or higher than those reported in literature for much thinner membranes.[8,37] Despite the thickness (81 μm) of these membranes, high permeance values were obtained, and this fast solvent transport can be attributed to the relatively large pore size of the membranes. These permeance studies show that the high retention of the membranes is not being achieved at the cost of water transport across the membrane.

As BNOx showed great retention performance for Evans Blue, a more detailed investigation was carried out on the samples to determine the performance of it using two smaller dyes with different functionalities, which are often utilised in retention studies, Methyl Orange and Methylene Blue. The tests were performed in the same manner as the Evans Blue tests. Methyl Orange and Methylene Blue showed retentions of 99–100% – higher than those obtained when testing Evans Blue. This data can be found in Table S5† and the UV-Vis absorption spectra representing the retention is shown in Fig. 10. These retention studies indicate that these membranes are capable of retaining larger dye molecules, like Evans Blue, as well as smaller molecules, such as Methyl Orange and Methylene Blue. Images of the membranes after filtering Methyl Orange and Methylene Blue are shown in Fig. S8† and show a clear staining of the membranes due to retention of the dyes.

Layered h-BN is regarded as an analogue to graphene, with a similar electron arrangement, which makes BN, and thus BNOx, a π-system.[34,38] The dyes used in this work are aromatic

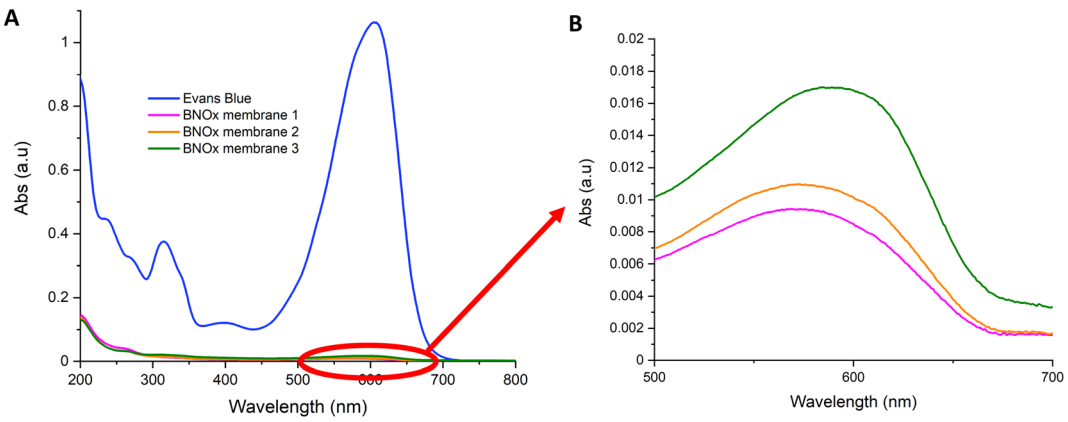


Fig. 9 (A) UV-Vis spectra of the retention of 20 mL of Evans Blue (15 μM) through BNOx membranes and (B) close-up of the absorbances of the absorbances of the permeates.

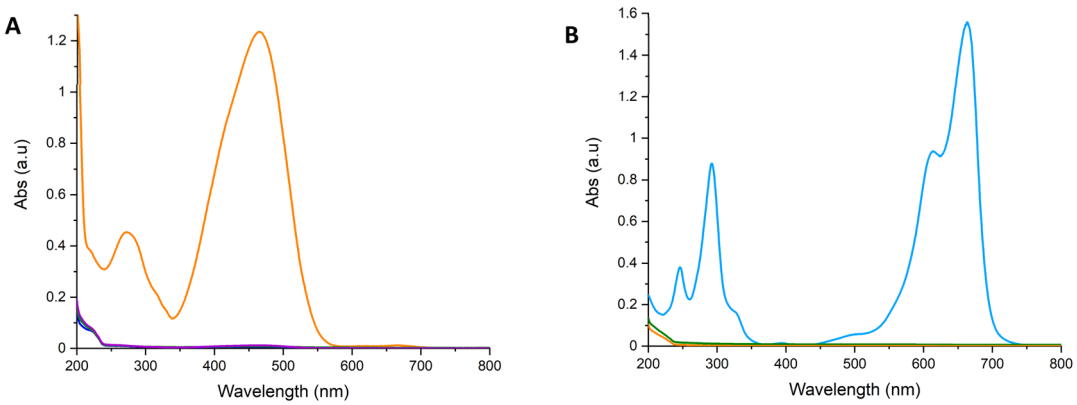


Fig. 10 UV-Vis spectra showing the retention of 20 mL of (A) Methyl Orange (50 μM), (B) Methylene Blue (27 μM) through BNOx membranes.

dyes and, therefore, have aromatic rings capable of interacting through π–π stacking with the BN rings.[39–41] Thus, the high retention of the dyes is due to physisorption and π–π stacking. The results obtained support this, as all three dyes are strongly retained by the membranes, regardless of the membrane pore size, and the size and charge of the dyes.

These performances show that the oxidation of the BN does not affect the formation of the membranes, keeping the outstanding performance observed for the BN membranes.[26] In fact, the membranes formed with the oxidised BN showed slightly higher mean retentions than those obtained with regular BN. This indicates that the oxidation already offers an advantage in comparison with regular BN, improving the retention of the membranes. Moreover, this oxidised BN can be further exploited in the future to functionalise the BNOx based membranes with various molecules. The facile B–OH bond functionalisation may open a unique approach for the production of new membranes for the separation of various molecules, such as mono-from di- and polysaccharides, as well as offering the potential of improving membrane integrity through cross-linking.

## 4. Conclusions

Oxidation of BN was successfully achieved by heating the BN powder in air at 1000 °C, obtaining BNOx. FT-IR and XRD characterisation of the BNOx sample showed the presence of OH groups, with the results being very similar to that of boric acid, further proving the oxidation of the BN. The nanosheets and membranes obtained were very similar to the BN ones, indicating that the oxidation doesn't change the morphology of the exfoliated material or formation of the membranes. This BNOx method was proven to be an easy and fast way to introduce functionalisation (OH groups) in BN. This functionalisation could be used for further modifications for several potential applications, including cross-linking and enantiomeric separation. BN can be oxidised with ease in a furnace, with the formation of OH groups starting at 700 °C, and it has been shown that additional oxidation can be achieved by sonicating the BNOx in water. This sonication results in both the exfoliation of the BN material as well introducing more OH into the BN structure, producing B–OH groups at the edges.

The membranes were tested for the three common dyes, exhibiting excellent retention performances, very similar to those obtained with the BN membranes. In addition, the membranes were shown to exhibit rapid solvent permeance, both for pure water and with Evans Blue aqueous solution. All of this seems to indicate that the oxidation does not negatively affect the performance of the membranes, that opens up the possibility to use this approach as a route for further functionalisation of the nanomaterial.

## Author contributions

Conceptualization, YKG; methodology, YKG, NGD and FPM; formal analysis, ÁC, ASA, MBC, AR, KM and PD; investigation, NGD, ÁC and M-LCG; resources, YKG; data curation, NGD, ÁC and FP-M; graphical abstract, ÁC; writing – original draft preparation, NGD, ÁC and YKG; writing – review and editing, NGD, ÁC, FP-M, and YKG; supervision, YKG, FP-M, KM and PD; project administration, YKG; funding acquisition, YKG. All authors have read and agreed to the published version of the manuscript.

## Conflicts of interest

There are no conflicts to declare.

## Acknowledgements

The authors would like to gratefully acknowledge Science Foundation Ireland and BiOrbic Bioeconomy Research Centre (grant number SFI 16/RC/3889) and Irish Research Council (grant number GOIPG/2019/2788) for financial support.

## Notes and references

1 Y. Du, B. K. Pramanik, Y. Zhang, L. Dumée and V. Jegatheesan, Recent Advances in the Theory and Application of Nanofiltration: a Review, *Curr. Pollut. Rep.*, 2022, **8**, 51–80.

2 P. Eriksson, Nanofiltration extends the range of membrane filtration, *Environ. Prog.*, 1988, **7**, 58–62.
3 N. García Doménech, F. Purcell-Milton and Y. K. Gun'ko, Recent progress and future prospects in development of advanced materials for nanofiltration, *Mater. Today Commun.*, 2020, **23**, 100888.
4 H. Liu, M. Zhang, H. Zhao, Y. Jiang, G. Liu and J. Gao, Enhanced dispersibility of metal–organic frameworks (MOFs) in the organic phase via surface modification for TFN nanofiltration membrane preparation, *RSC Adv.*, 2020, **10**, 4045–4057.
5 A. A. Khan, H. A. Maitlo, I. A. Khan, D. Lim, M. Zhang, K. H. Kim, J. Lee and J. O. Kim, Metal oxide and carbon nanomaterial based membranes for reverse osmosis and membrane distillation: A comparative review, *Environ. Res.*, 2021, **202**, 111716.
6 S. Gao, Y. Zhu, Y. Gong, Z. Wang, W. Fang and J. Jin, Ultrathin Polyamide Nanofiltration Membrane Fabricated on Brush-Painted Single-Walled Carbon Nanotube Network Support for Ion Sieving, *ACS Nano*, 2019, **13**, 5278–5290.
7 D. Liu, L. He, W. Lei, K. D. Klika, L. Kong and Y. Chen, Multifunctional Polymer/Porous Boron Nitride Nanosheet Membranes for Superior Trapping Emulsified Oils and Organic Molecules, *Adv. Mater. Interfaces*, 2015, **2**, 1500228.
8 C. Chen, J. Wang, D. Liu, C. Yang, Y. Liu, R. S. Ruoff and W. Lei, Functionalized boron nitride membranes with ultrafast solvent transport performance for molecular separation, *Nat. Commun.*, 2018, **91**(9), 1–8.
9 W. Lei, D. Portehault, D. Liu, S. Qin and Y. Chen, Porous boron nitride nanosheets for effective water cleaning, *Nat. Commun.*, 2013, **41**(4), 1–7.
10 Z. Cui, A. J. Oyer, A. J. Glover, H. C. Schniepp and D. H. Adamson, Large Scale Thermal Exfoliation and Functionalization of Boron Nitride, *Small*, 2014, **10**, 2352–2355.
11 F. Xiao, S. Nafi cy, G. Casillas, M. H. Khan, T. Katkus, L. Jiang, H. Liu, H. Li, Z. Huang, F. Xiao, M. H. Khan, T. Katkus, H. Liu, Z. Huang, S. Nafi cy, G. Casillas, L. Jiang and H. Li, Edge-Hydroxylated Boron Nitride Nanosheets as an Effective Additive to Improve the Thermal Response of Hydrogels, *Adv. Mater.*, 2015, **27**, 7196–7203.
12 Y. Andriani, J. Song, P. C. Lim, D. H. L. Seng, D. M. Y. Lai, S. L. Teo, J. Kong, X. Wang, X. Zhang and S. Liu, Green and efficient production of boron nitride nanosheets via oxygen doping-facilitated liquid exfoliation, *Ceram. Int.*, 2019, **45**, 4909–4917.
13 R. Moradian and S. Azadi, Magnetism in defected single-walled boron nitride nanotubes, *Europhys. Lett.*, 2008, **83**(1), 17007.
14 J. Wu and W. Zhang, Tuning the magnetic and transport properties of boron-nitride nanotubes via oxygen-doping, *Solid State Commun.*, 2009, **149**, 486–490.
15 R. S. Singh, Influence of oxygen impurity on electronic properties of carbon and boron nitride nanotubes: A comparative study, *AIP Adv.*, 2015, **5**, 117150.
16 J. W. Feng, Y. J. Liu and J. X. Zhao, Theoretical prediction of the mechanisms for defect healing or oxygen doping in a hexagonal boron nitride (h-BN) sheet with nitrogen vacancies by NO2 molecules, *J. Mol. Model.*, 2014, **20**, 1–7.
17 A. Tokarev, E. Kjeang, M. Cannon and D. Bessarabov, Theoretical limit of reversible hydrogen storage capacity for pristine and oxygen-doped boron nitride, *Int. J. Hydrogen Energy*, 2016, **41**, 16984–16991.
18 Q. Weng, D. G. Kvashnin, X. Wang, O. Cretu, Y. Yang, M. Zhou, C. Zhang, D.-M. Tang, P. B. Sorokin, Y. Bando, D. Golberg, Q. Weng, O. Cretu, M. Zhou, C. Zhang, D.-M. Tang, Y. Bando, D. Golberg, D. G. Kvashnin, P. B. Sorokin, X. Wang and Y. Yang, Tuning of the Optical, Electronic, and Magnetic Properties of Boron Nitride Nanosheets with Oxygen Doping and Functionalization, *Adv. Mater.*, 2017, **29**, 1700695.
19 J. Li, P. Jin, W. Dai, C. Wang, R. Li, T. Wu and C. Tang, Excellent performance for water purification achieved by activated porous boron nitride nanosheets, *Mater. Chem. Phys.*, 2017, **196**, 186–193.
20 J. Xiong, L. Yang, Y. Chao, J. Pang, M. Zhang, W. Zhu and H. Li, Boron Nitride Mesoporous Nanowires with Doped Oxygen Atoms for the Remarkable Adsorption Desulfurization Performance from Fuels, *ACS Sustainable Chem. Eng.*, 2016, **4**, 4457–4464.
21 L. H. Li, J. Cervenka, K. Watanabe, T. Taniguchi and Y. Chen, Strong oxidation resistance of atomically thin boron nitride nanosheets, *ACS Nano*, 2014, **8**, 1457–1462.
22 B. Yu, W. Xing, W. Guo, S. Qiu, X. Wang, S. Lo and Y. Hu, Thermal exfoliation of hexagonal boron nitride for effective enhancements on thermal stability, flame retardancy and smoke suppression of epoxy resin nanocomposites: Via sol-gel process, *J. Mater. Chem. A*, 2016, **4**, 7330–7340.
23 G. R. Bhimanapati, D. Kozuch and J. A. Robinson, Large-scale synthesis and functionalization of hexagonal boron nitride nanosheets, *Nanoscale*, 2014, **6**, 11671–11675.
24 T. Sainsbury, A. Satti, P. May, Z. Wang, I. McGovern, Y. K. Gun'ko and J. Coleman, Oxygen radical functionalization of boron nitride nanosheets, *J. Am. Chem. Soc.*, 2012, **134**, 18758–18771.
25 Y. Guo and W. Guo, Hydroxylation of a metal-supported hexagonal boron nitride monolayer by oxygen induced water dissociation, *Phys. Chem. Chem. Phys.*, 2015, **17**, 16428–16433.
26 N. G. Doménech, F. Purcell-Milton, A. S. Arjona, M.-L. C. García, M. Ward, M. B. Cabré, A. Rafferty, K. McKelvey, P. Dunne and Y. K. Gun'ko, High-Performance Boron Nitride Based Membranes for Water Purification, *Nanomater*, 2022, **12**, 473.
27 L. Sun, H. Huang and X. Peng, Laminar $MoS_2$ membranes for molecule separation, *Chem. Commun.*, 2013, **49**, 10718.
28 Z. Liu, J. Li and X. Liu, Novel Functionalized BN Nanosheets/Epoxy Composites with Advanced Thermal Conductivity and Mechanical Properties, *ACS Appl. Mater. Interfaces*, 2020, **12**, 6503–6515.
29 W. Zhu, X. Gao, Q. Li, H. Li, Y. Chao, M. Li, S. M. Mahurin, H. Li, H. Zhu and S. Dai, Controlled Gas Exfoliation of Boron

Nitride into Few-Layered Nanosheets, *Angew. Chem., Int. Ed.*, 2016, **55**, 10766–10770.

30 B. Yu, W. Xing, W. Guo, S. Qiu, X. Wang, S. Lo and Y. Hu, Thermal exfoliation of hexagonal boron nitride for effective enhancements on thermal stability, flame retardancy and smoke suppression of epoxy resin nanocomposites: Via sol-gel process, *J. Mater. Chem. A*, 2016, **4**, 7330–7340.

31 K. Nakamoto, in *Infrared and Raman Spectra of Inorganic and Coordination Compounds*, John Wiley & Sons, Inc., 2009, pp. 149–354.

32 X. Shen, X. Lin, N. Yousefi, J. Jia and J. K. Kim, Wrinkling in graphene sheets and graphene oxide papers, *Carbon*, 2014, **66**, 84–92.

33 S. Tosoni, K. Doll and P. Ugliengo, Hydrogen Bond in Layered Materials: Structural and Vibrational Properties of Kaolinite by a Periodic B3LYP Approach, *Chem. Mater.*, 2006, **18**, 2135–2143.

34 Y. Lin, T. V Williams, T.-B. Xu, W. Cao, H. E. Elsayed-Ali and J. W. Connell, Aqueous Dispersions of Few-Layered and Monolayered Hexagonal Boron Nitride Nanosheets from Sonication-Assisted Hydrolysis: Critical Role of Water, *J. Phys. Chem. C*, 2011, **115**, 2679–2685.

35 E. S. Tarleton, J. P. Robinson, C. R. Millington, A. Nijmeijer and M. L. Taylor, The influence of polarity on flux and rejection behaviour in solvent resistant nanofiltration—Experimental observations, *J. Membr. Sci.*, 2006, **278**, 318–327.

36 L. H. Li and Y. Chen, Atomically Thin Boron Nitride: Unique Properties and Applications, *Adv. Funct. Mater.*, 2016, **26**, 2594–2608.

37 R. Das, P. Solís-Fernández, D. Breite, A. Prager, A. Lotnyk, A. Schulze and H. Ago, High flux and adsorption based non-functionalized hexagonal boron nitride lamellar membrane for ultrafast water purification, *Chem. Eng. J.*, 2021, **420**, 127721.

38 T. Greber, Graphene and Boron Nitride Single Layers, *Handbook of Nanophysics: Functional Nanomaterials*, 2009, pp. 18-1–18-22.

39 Y. Xue, P. Dai, X. Jiang, X. Wang, C. Zhang, D. Tang, Q. Weng, X. Wang, A. Pakdel, C. Tang, Y. Bando and D. Golberg, Template-free synthesis of boron nitride foam-like porous monoliths and their high-end applications in water purification, *J. Mater. Chem. A*, 2016, **4**, 1469–1478.

40 A. Hafeez, Z. A. Karim, A. F. Ismail, A. Samavati, K. A. M. Said and S. Selambakkannu, Functionalized boron nitride composite ultrafiltration membrane for dye removal from aqueous solution, *J. Memb. Sci.*, 2020, **612**, 118473.

41 D. Liu, W. Lei, S. Qin and Y. Chen, Template-Free Synthesis of Functional 3D BN architecture for removal of dyes from water, *Sci. Rep.*, 2014, **4**, 1–5.